Composites: Part A 73 (2015) 20–34

Contents lists available at ScienceDirect

Composites: Part A

journal homepage: www.elsevier.com/locate/compositesa

Experimental study on delamination migration in composite laminates

Maria Francesca Pernice [a,*], Nelson V. De Carvalho [b], James G. Ratcliffe [c], Stephen R. Hallett [a]

[a] Advanced Composite Centre for Innovation and Science (ACCIS), University of Bristol, Bristol BS8 1TR, UK
[b] National Institute of Aerospace, resident at: Durability, Damage Tolerance and Reliability Branch, NASA Langley Research Center, Hampton, VA 23681-2199, USA
[c] Durability, Damage Tolerance and Reliability Branch, NASA Langley Research Center, Hampton, VA 23681-2199, USA

ARTICLE INFO

Article history:
Received 11 November 2014
Received in revised form 28 January 2015
Accepted 21 February 2015
Available online 28 February 2015

Keywords:
B. Delamination
B. Transverse cracking
D. Mechanical testing
C. Finite element analysis (FEA)

ABSTRACT

The transition of delamination growth between different ply interfaces in composite tape laminates, known as migration, was investigated experimentally. The test method used promotes delamination growth initially along a $0/\theta$ ply interface, which eventually migrates to a neighbouring $\theta/0$ ply interface. Specimens with $\theta = 60°$ and $75°$ were tested. Migration occurs in two main stages: (1) the initial $0/\theta$ interface delamination turns, transforming into intraply cracks that grow through the θ plies; this process occurs at multiple locations across the width of a specimen, (2) one or more of these cracks growing through the θ plies reaches and turns into the $\theta/0$ ply interface, where it continues to grow as a delamination. A correlation was established between these experimental observations and the shear stress sign at the delamination front, obtained by finite element analyses.

Overall, the experiments provide insight into the key mechanisms that govern delamination growth and migration.

1. Introduction

Historically, delamination in composite laminates has been treated as an individual damage mechanism. Numerous test methods have been developed for characterizing delamination. The majority of these methods have common features such as enforcement of delamination initiation and growth at a single unidirectional ply interface and the use of the critical strain energy release rate for defining a laminate's interlaminar fracture toughness [1,2]. This has led to several testing standards for characterizing delamination under quasi-static and cyclic loading conditions [3–5]. Analysis methods have been developed based on linear elastic fracture mechanics and utilize the measurements of fracture toughnesses obtained from these standardized tests as the criterion for delamination growth [6,7]. Combined, these experimental and analytical efforts have led to significant advances towards a practical means for assessing the damage tolerance of composite structures from a fracture mechanics perspective.

Failure of composite structure involving delamination, however, typically involves multiple delamination cracks, which often grow and migrate into different ply interfaces. This behaviour has been documented in several cases, including low-velocity impact [8], skin/stiffener debonding [9], delamination growth from embedded defects and notches [10–12] and non-unidirectional laminates under shear [13]. Hence, recent work has focused on accounting for this behaviour to a level suitable for more realistic delamination growth prediction. For instance, enhancements to traditional engineering analysis frameworks, such as the extended [14] and augmented [15] finite element methods and the phantom node [16] and floating node [17] methods may provide a practical means of simulating damage mechanisms such as delamination migration, as in [18], which combines the extended finite element method and the cohesive elements approach. However, these methods still require knowledge of the fundamental driving mechanisms for delamination propagation and migration at non-unidirectional ply interfaces.

In the literature, two different mechanisms leading to perceived delamination relocation to a different ply interface are described. In [11,19], delamination was reported to propagate through the thickness of a laminate by "joining up with" or "migrating" through pre-existing ply splits, which were caused by the global loading conditions on the laminate. Other studies [20–22] observed delamination relocation to other ply interfaces through a process by which delamination "propagates out" or "*kinks out*" of the original interface into one of the bounding plies, without the necessary presence of pre-existing ply splits. This process was also observed in [19], together with the first mechanism described, of delaminations migrating through pre-existing ply splits.

* Corresponding author. Tel.: +44 117 33 15 513.
E-mail address: aemfp@my.bristol.ac.uk (M.F. Pernice).

http://dx.doi.org/10.1016/j.compositesa.2015.02.018
1359-835X/

The present work focuses on the study of the second mechanism, by which delamination turns out of the original interface into one of the bounding plies, hereafter referred to as ''delamination migration.'' Following the terminology used in [23], in the present work the turning of a delamination into one of the adjacent plies is referred to as ''kinking''. The term ''migration'' is used to refer to the complete process, by which a delamination propagating at an interface relocates to another interface. Delamination kinking, and subsequent migration, can be explained by the micromechanism of crack formation leading to delamination. Delamination is the result of the coalescence of microcracks formed at a ply interface, perpendicular to the resolved tensile stress [20,24,25]. Under pure shear or mixed-mode loading conditions, the resolved tensile stress is oriented out of the laminate plane. Consequently, the microcracks are angled with respect to the laminate plane and the resulting delamination tends to propagate out of the plane of the interface, through the thickness of a laminate [20,26]. The orientation of the resolved tensile stress at the delamination front determines which of the interfacing plies the microcracks are driven towards. If the fibre orientation in this ply precludes containment of the microcracks, migration occurs [20,26]. If, instead, the fibres are aligned and can block intralaminar fracture, then delamination stays at the interface, and propagates along the fibre direction, as demonstrated experimentally in [19,21,22].

The mechanism by which delamination gradually kinks out of an interface into a ply and migrates to a neighbouring interface was investigated and explained in detail for a 0/90 ply interface in [21]. The work describes a new experimental test method, specifically intended for investigating the fundamental mechanisms driving delamination migration. The test allowed the isolation of a single delamination migration event, enabling detailed study of the migration process. This was achieved by the test configuration, which causes a reversal in the shear stress sign at the delamination front during specimen loading, so that delamination propagates at a 0/90 interface before kinking through a stack of four 90° plies and migrating to a neighbouring interface. The study involved cross-ply specimens, in order to obtain uniform delamination migration across the specimen width, creating a benchmark for advanced modelling techniques [27]. However, tests conducted in [21] offer only partial insight into migration in general stacking sequences, due to the focus on cross-ply specimens. Delamination growth in actual composite structures at other ply interfaces may involve mechanisms that differ from those observed in [21].

The objective of the present work was to investigate delamination migration at other 0/θ interfaces. To this end, the cross-ply migration specimen was modified to study delamination at 0/60 and 0/75 ply interfaces. The specimen stacking sequence was modified to reduce coupling effects arising from the non-symmetric 0/θ interface. Damage progression was monitored by an X-ray Computed Tomography technique. The shear stress sign reversal at the delamination front in the specimen was evaluated by finite element analyses with the aim of qualitatively interpreting experimental observations.

2. Experimentation

2.1. Delamination migration test

The delamination migration test was proposed in [21]. A schematic representation of the test is given in Fig. 1a, together with an illustration of the setup in Fig. 1b. The original specimen consists of a cross-ply layup, with a polytetrafluoroethylene (PTFE) film insert at an interface between a 0° ply (specimen length direction) and a stack of four 90° plies, Fig. 2a. The specimen layup, shown in Fig. 2a, was obtained by modifying a baseline layup [21] such that near the PTFE film plane a sequence 0/T/90_4/0 is obtained. The test fixture is comprised of an adjustable, rigid baseplate that enables precise specimen alignment, and variation of the load offset L, Fig. 1a. The specimen is positioned and clamped at both ends on the baseplate. A 15 mm-long section of the upper arm of the specimen (in the delaminated portion) is removed to allow clamping of the lower arm on the test fixture. Specimens are loaded on the upper surface in displacement control at quasi-static loading rates via the piano hinge assembly pictured in Fig. 1b.

The test functions on the premise that the propensity for kinking of a delamination into the ply below or above a given interface can be controlled by varying the sign of the shear stress acting at the delamination front. In the context of the test specimen depicted in Fig. 1, when the delamination length, a, is less than the load offset, L, the shear stress acts as indicated in Fig. 3a. Therefore, the resolved principal tensile stress tends to drive delamination towards the lower 0° ply, fibres of which prevent crack growth through the ply, yielding delamination growth along the 0/90 ply interface. The shear stress sign reverses shortly after delamination growth proceeds past the load-application point (Fig. 3b). The delamination is now driven towards the upper 90° ply stack (Fig. 3b), where fibres are unable to contain crack growth through the stack. This ultimately leads to delamination kinking into this ply stack and eventually migrating to another ply interface. Finally, the presence of the 0° ply, above the 90° ply stack, prevents further migration events through the thickness. Additionally, it is worth noting that L can control the initial sign of the shear stress. If L is made smaller than the initial delamination length, a_0, the shear stress will act as indicated in Fig. 3b immediately favouring migration into the 90° ply stack from the onset.

In the cross-ply specimen [21], the shear stress sign reversal at the delamination front occurs uniformly across the specimen width, assuring a uniform delamination migration event, which can be monitored from the specimen edges. Specimens in the current study expand upon this testing method by considering migration at two different ply interfaces. Details of these new specimens and testing practices are provided in the following sections.

2.2. Specimens and fabrication

A new stacking sequence (depicted in Fig. 2b) was designed for the delamination migration specimen, in order to investigate delamination migration at a 0/θ interface. The fibre orientations, θ, studied were 60° and 75°, chosen to have equi-spaced angles from the original 90° fibre orientation towards the 0° direction used in standard fracture testing. Similar to the original layup, the new layup was obtained from a baseline stacking sequence, which was then modified by repositioning two 0° plies (shown in Fig. 2b) to obtain a stacking sequence 0/T/θ_4/0 near the PTFE film. The lower 0° ply near the PTFE film enables delamination at the initial 0/θ interface at the beginning of the test, where the shear stress acts as in Fig. 3a. Once the shear sign changes, the delamination may kink into the θ-oriented ply stack. Delamination migration occurs once the kinked crack reaches the upper 0° bounding ply, transitioning into a delamination that grows along the upper θ/0 interface. Classical laminated plate theory [28] was used to select a layup suitable for the test and which minimized unwanted coupling effects. The number of plies in the stacking sequence was increased to 56, from the original 44-ply layup of [21], to minimize coupling effects arising from the central non-symmetric stacking sequence. Extension/bending coupling was kept low to reduce thermal distortions during curing. Bending/twisting coupling needed to be minimized, to avoid its unwanted effect on delamination-front loading conditions. Bending/twisting coupling was

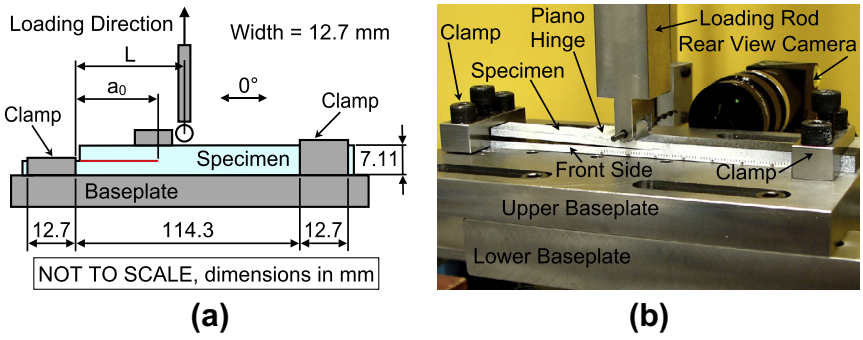

Fig. 1. Schematic of the delamination migration test setup (a) and specimen in the test fixture (b) (Adapted from [21]).

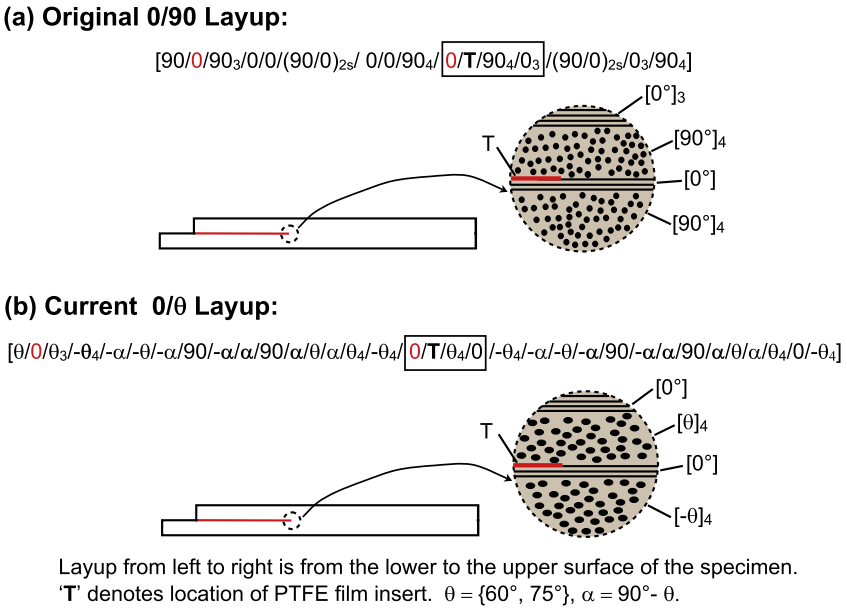

Fig. 2. Comparison between (a) the original cross-ply stacking sequence used in [21] and (b) the new 0/θ stacking sequence employed in the present work. Plies sequence from left to right is from the lower to the upper surface of the specimen.

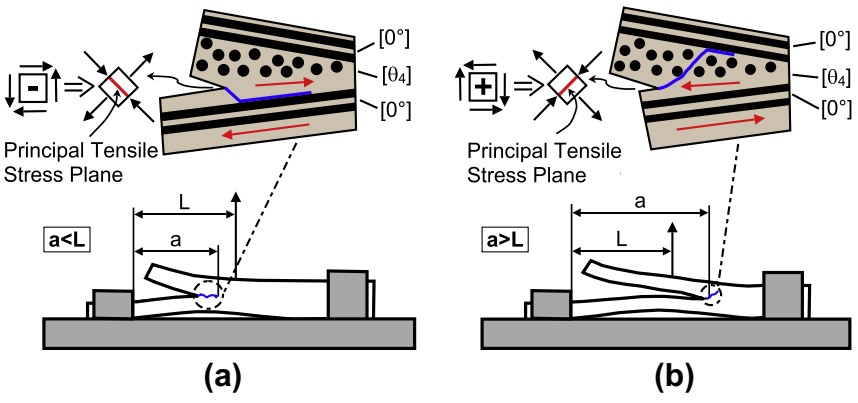

Fig. 3. Effect of shear stress sign at the delamination front at different stages of delamination growth (Redrawn from [21]).

evaluated by the ratio D_{16}/D_{11} [29,30] between terms of the bending stiffness matrix D (as defined in [28]). In the complete laminate (lower + upper sublaminates) and in the lower sublaminate, D_{16}/D_{11} was less than 0.5% for both fibre orientations tested. The upper sublaminate is balanced and anti-symmetric, and therefore does not exhibit bending/twisting coupling.

A 326 mm-square panel of each fibre orientation ($\theta = 60°$ and 75°) comprised of IM7/8552 carbon-epoxy tape was manufactured. The material used had a nominal ply thickness of 0.127 mm. Each plate contained a central 136 mm-wide strip of 12.7 μm-thick PTFE film, acting as the initial delamination in the specimens. The two plates were cured in an autoclave, according to the curing cycle recommended by the material manufacturer [31]. Each plate was cut in half across the PTFE insert to obtain an initial artificial delamination in the specimens. The specimens were nominally 12.7 mm-wide, 145 mm-long and 7.11 mm-thick, with an initial delamination length, a_0 (Fig. 1a), equal to 53 mm.

2.3. Test procedure

The edges of each specimen were covered with a thin layer of white paint to better visualize delamination growth and kinking during the tests. A calibrated scale was also applied to each edge in order to help monitor delamination growth and migration position. Tests were conducted using a hydraulic load frame equipped with a 22 kN load cell. Specimens were loaded in displacement control, at a rate of 0.127 mm/min. Specimens were unloaded (at the same rate) after a predetermined amount of delamination growth and/or migration had occurred. Applied load and machine crosshead displacement were recorded throughout each test.

Tests were performed with load offsets $L = \{0.35a_0, 1.0a_0, 1.1a_0, 1.2a_0, 1.3a_0\}$, with $a_0 = 53$ mm. Two test procedures were adopted: single-step and incremental. In the single-step tests, specimens were loaded until either migration was observed on both lateral edges of the specimen, or a maximum delamination length of 40 mm from the PTFE insert front was reached. In the incremental tests, loading of the specimens was stopped at significant events, such as load drops or delamination kinking, previously observed during the single-step tests, as described in Section 4. The specimens were then unloaded and removed from the test fixture, inspected and then repositioned in the test fixture for the next loading step. Incremental tests provided insight into the sequence of damage events inside the specimen prior to delamination migration.

2.4. Test matrix

At least four specimens were tested with each load offset for each fibre angle. Incremental tests were performed on specimens with load offset $L = 1.0a_0$ and $L = 0.35a_0$. The results obtained from specimens tested with a load offset $L = 1.0a_0$ are thought to be representative of the results from all the cases during which delamination growth from the PTFE insert front is promoted prior to migration ($L = \{1.0a_0, 1.1a_0, 1.2a_0, 1.3a_0\}$). Incremental tests on specimens with load offset $L = 0.35a_0$ were also conducted, to investigate the other failure sequence tested, during which migration occurs from the onset at the PTFE insert front. Table 1 shows details of the total number of specimens tested and the number of incremental tests, indicated in parenthesis.

2.5. Inspection methods

Delamination growth and migration were monitored during the test using a camera on each side of the specimen synchronized with a specimen's force–displacement response. The views from the edge cameras are referred to as "front side view" and "rear side view". The front side is the side visible in Fig. 1b, such that delamination propagates from left to right. Specimens were inspected using X-ray Computed Tomography (CT scan) scanning. Fracture surfaces of specimens completely tested were inspected using a Philips XC30 Scanning Electron Microscope (SEM) with an acceleration voltage of 20 kV. In preparation for SEM inspection, 2–3 nm of gold plating was sputtered onto the specimens' surfaces.

Table 1
Total number of specimens tested for each fibre angle, θ, and load offset, L. Number in parenthesis indicates number of specimens tested incrementally.

	Loading position L/a_0				
θ	0.35	1.0	1.1	1.2	1.3
60°	5 (1)	9 (5)	4	4	4
75°	4 (1)	7 (1)	4	4	4

3. Numerical model

Finite element analyses were performed to qualitatively interpret and support the experimental observations. A correlation was found between the delamination migration location observed in the experimental tests and the shear stress sign reversal at the delamination front in the finite element analysis. Analyses were performed of specimens with 0/90 interface tested in [22] and of specimens with 0/75 and 0/60 interfaces tested in this work, using the commercial code ABAQUS/Standard, version 6.12 [32].

For each specimen type, a 3D solid model of a specimen of total length 139.7 mm and width of 12.7 mm was created using ABAQUS CAE. One layer of eight-node brick elements (ABAQUS type C3D8) was used for each ply in the stacking sequence, assuming a ply thickness of 0.127 mm and the number of plies given by the specific stacking sequence. The model used to investigate the specimen with 0/75 and 0/60 interfaces tested in this work is shown in Fig. 4. Details regarding layup and dimensions of the cross-ply specimen are given in [22] and are omitted here for brevity. A refined mesh was used in the four plies closer to the delaminated interface, where element length was halved and was equal to 0.3125 mm. The mesh was also refined at the specimen lateral edges, to account for possible edge effects, with elements width ranging from 0.3175 mm to 0.6207 mm. The orthotropic material properties for IM7/8552 were taken from [33]: $E_{11} = 161.0$ GPa, $E_{22} = E_{33} = 11.38$ GPa, $\upsilon_{12} = \upsilon_{13} = 0.32$, $\upsilon_{23} = 0.436$, $G_{12} = G_{13} = 5.17$ GPa, $G_{23} = 3.98$ GPa. A 12.7 mm long section at both ends of the specimen was constrained by fixing all the translational degrees of freedom on the top and bottom surfaces, to simulate idealized clamping conditions in the test fixture, resulting in a specimen length of 114.3 mm between the clamps. Load was applied as a fixed vertical displacement of 1 mm to simulate the displacement controlled test conditions. Boundary conditions applied to the model are depicted in Fig. 4. Analyses were conducted with the load-application point coincident with the PTFE insert front ($L = a_0$, Fig. 4). The initial delamination was modelled using elements with coincident nodes at the $0/\theta$ interface. The intact portion of the specimen was modelled by applying a multipoint constraint to the nodes at the interface. The main goal of the model was to investigate the variation of the shear stress sign across the delamination front with increasing delamination length. To simplify the analyses, a straight delamination front in the direction of the specimen width (90° direction) was assumed, which does not precisely reflect the exact experimental conditions. However, this assumption is believed to be acceptable to obtain qualitative results, because of the observed negligible curvature of the delamination front in these specimens prior to migration (as shown in the X-ray CT images in Section 4.2.1). Ten linear analyses

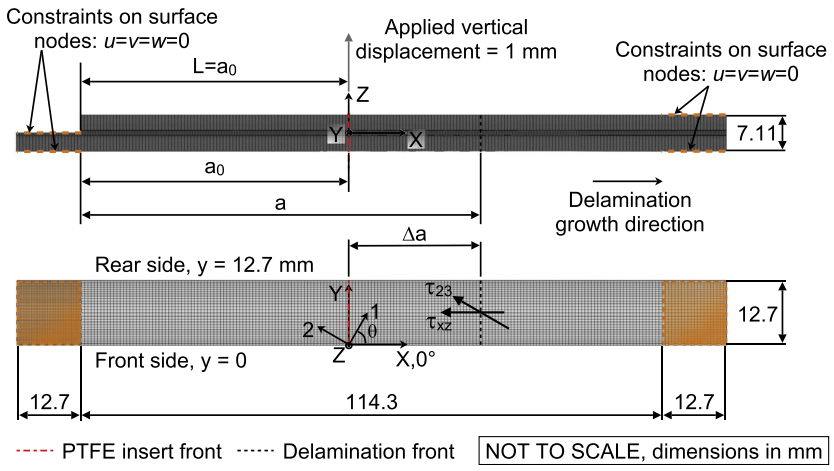

Fig. 4. Finite element model of the delamination migration specimen with dimensions and boundary conditions.

were conducted, first assuming an initial delamination length equal to a_0 and then increasing the delamination length by a distance Δa equal to 2.5, 5, 7.5, 10, 12.5, 15, 20, 30 and 35 mm. Fig. 4 gives an example of the location of the delamination front along the specimen, at a distance Δa from the PTFE insert front.

4. Results and discussion

4.1. Numerical results

Based on the work presented in [21], kinking in the delamination migration specimens is assumed to be related to the sign of the component of shear stress, τ_{23}, perpendicular to the fibres in the upper θ-oriented ply stack at the delaminating interface. In the original cross-ply specimens [21], τ_{23} corresponds to the global shear stress component τ_{xz}, illustrated in Fig. 4. At a $0/\theta$ interface, the local shear stress, τ_{23}, is oriented as in Fig. 4. For each analysis, τ_{23} was plotted against the distance y along the delamination front, in the specimen width direction, going from the front edge, $y = 0$, to the rear edge, $y = 12.7$ mm (Fig. 4), to evaluate the delamination length, Δa, at which sign reversal occurs.

Results are shown in Fig. 5 for each specimen modelled, at a delamination length $\Delta a = 0$, 2.5, 5 and 7.5 mm. In Fig. 5, the shear stress component τ_{23} is normalized by the absolute value of shear stress in the centre of the specimen at the delamination length equal to a_0, $|\tau_{23,c}|$, indicated in Fig. 5. This normalization was performed to evaluate the sign of the shear stress at the delamination front, regardless of its magnitude. It is assumed that a negative sign of shear stress promotes delamination growth at the $0/\theta$ interface (Fig. 3a), while a positive sign promotes kinking of the delamination into the upper θ_4 ply stack (Fig. 3b). Fig. 5 shows that, for each θ, shear stress is negative, and therefore delamination growth is favoured, at the beginning of the test ($\Delta a = 0$ mm) and becomes positive, favouring kinking, when the delamination length increases. The plots in Fig. 5a show that, at a 0/90 interface, the shear stress τ_{23} (equivalent to τ_{xz} in this case) is uniform across the specimen width and shear stress sign reversal occurs uniformly at the same delamination length. By contrast, at a $0/\theta$ interface, the distribution of shear stress at the delamination front varies across the specimen width, depending upon the fibre angle, as depicted in Fig. 5b for the 0/75 interface and more clearly in Fig. 5c for the 0/60 interface. Consequently, the shear stress sign reverses at different delamination lengths across the specimen width at a $0/\theta$ interface. This result is highlighted in Fig. 6, which shows the variation of shear stress with increasing delamination length in three points across the delamination front, at a distance from the front edge of the specimen y equal to 1/8, 1/2 and 7/8 of the specimen width, W. In the case of the 0/90 interface, shear stress does not vary along the delamination front (the three curves in Fig. 6a are coincident). For the 0/75 interface, the delamination length at which shear stress sign reverses starts to differ, as it can be observed in the detail in Fig. 6b. This difference increases when the fibre angle, θ, decreases, as it is clearly visible in Fig. 6c for the 0/60 interface. Further details of the numerical results are discussed in relation to the interpretation of the experimental results, and are presented in what follows.

4.2. Experimental results

Test results for the two specimen types, containing 0/75 and 0/60 interfaces, are presented separately. Damage progression as obtained from incremental tests in specimens loaded at $L = a_0$ is reported as a reference case. The effect of changing the load offset is then presented. For each test configuration (specimen type and load offset, L) the specimen response was generally repeatable among duplicate tests, therefore for each case only a representative force–displacement curve is shown. X-ray CT scan images shown refer to a section parallel to the laminate plane taken at the θ-ply delamination surface at the $0/\theta$ interface, unless otherwise specified.

4.2.1. Loading point coincident with PTFE insert front

4.2.1.1. 0/75 ply interface. Representative single-step and incremental force–displacement responses of a specimen loaded at a location coincident with the PTFE insert front are shown in Fig. 7. For brevity, in Fig. 7, edge views at key stages during testing are shown only for the incremental test, as they were equivalent to the single-step tests. The force–displacement response was predominantly linear up to the maximum force (282 N in the single-step force–displacement curve, Fig. 7). At this point, an unstable event took place, corresponding to delamination growth onset and propagation (between 9 and 12 mm). A small amount of fibre bridging at the delamination onset at the PTFE insert front was observed from the edge views. Continued specimen loading yielded a combination of moderately stable delamination growth and kinking events (visible on the rear edge view), until delamination migration was completed (details of these processes are presented later in this Section). These kinking events involved a delamination turning upwards and propagating part way through the 75° ply stack, arresting, and propagating back to its original 0/75 ply interface. The kink angle, Ω, was measured as the angle between the

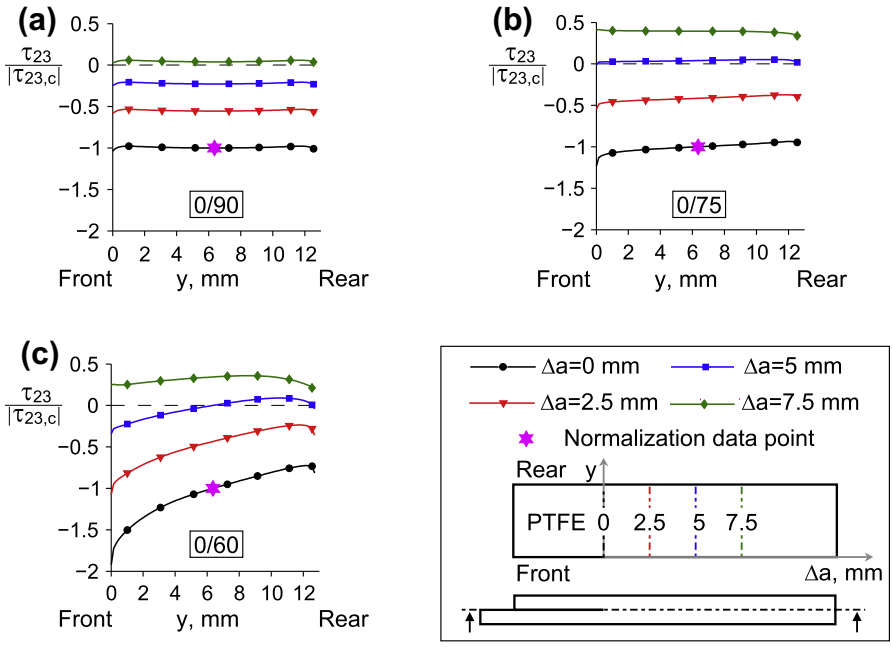

Fig. 5. Shear stress distribution along the specimen width at increasing delamination length, Δa, for the three interfaces modelled.

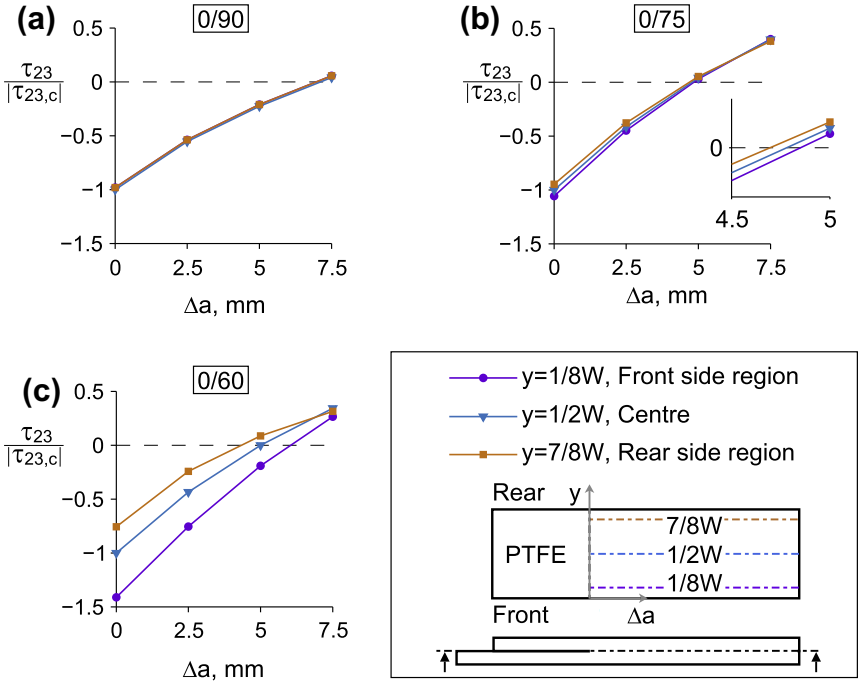

Fig. 6. Shear stress as function of the delamination length, Δa, at different locations in the specimen width for the three interfaces modelled.

horizontal line in the upper interface and the terminating linear section of the kinked crack, as shown in Fig. 7. Details of kink angle measurements are discussed at the end of this Section. Specimen unloading was slightly non-linear, resulting in a residual machine crosshead displacement of approximately 0.1 mm.

Details of progression of delamination and migration inside the specimen were obtained through incremental loading and X-ray CT scanning of specimens. A sequence of X-ray CT scan images taken after each of the three loading increments (labelled I, II and III, Fig. 7) is presented in Fig. 8. Fig. 8 shows that after initial delamination growth along the 0/75 interface (skimming the surface of the 0° ply), kinking initiated in the body of the specimen, in a region approximately between the centre and the rear edge of the specimen, (see Increment I: Points 1, 2 and 3, Fig. 8). At these locations, the delamination started to propagate close to, or just inside, the upper 75° ply at the interface or kinked through

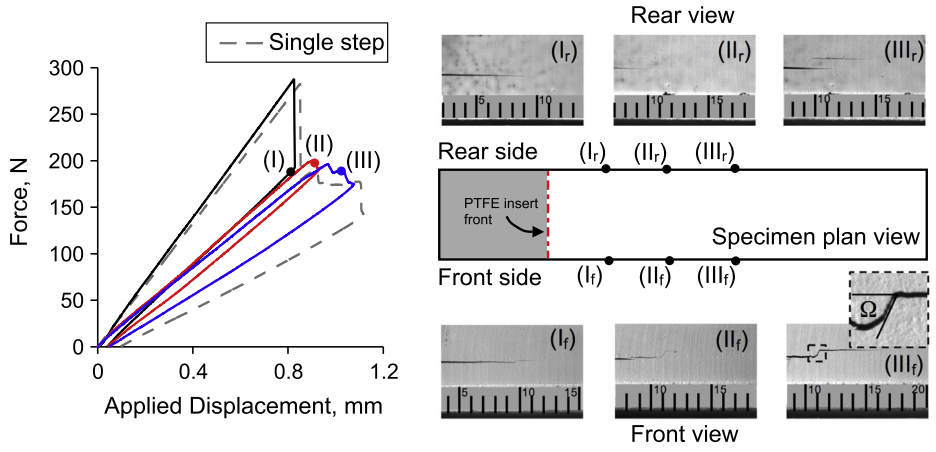

Fig. 7. Force–displacement response of specimens containing a 0/75 interface loaded at $L = a_0$ and edge views at key stages during the test, of the front edge of the specimen ("Front view") and the rear edge of the specimen ("Rear view").

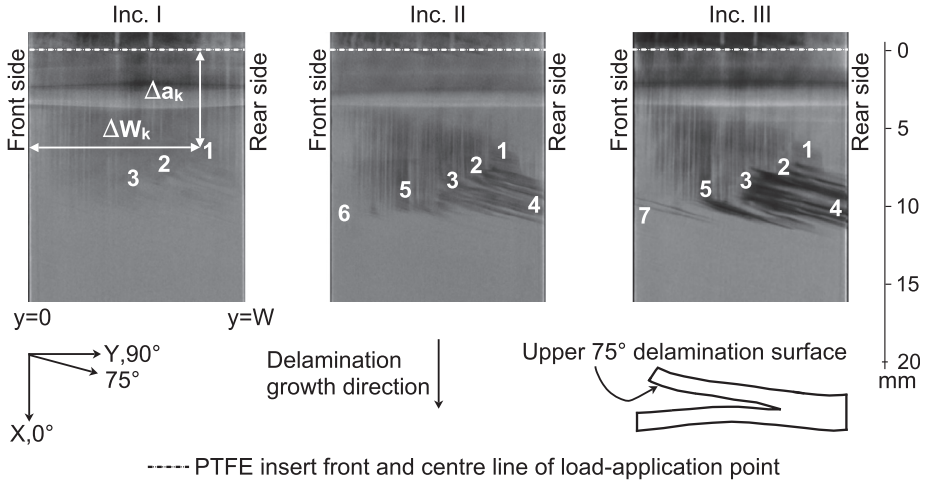

Fig. 8. Sequence of X-ray CT scan images of the upper delamination surface at the 0/75 interface resulting from incremental loading of a specimen.

the 75° ply stack. The resulting cracks propagated along the 75° fibre direction, towards the rear edge of the specimen, although they did not reach the rear edge at this stage of testing, which is confirmed by the Increment I edge views in Fig. 7. The initiation of kinking occurred at a distance ΔW_k from the front edge of the specimen ranging between 5 and 10 mm and a distance Δa_k from the load-application point ranging between 3.5 and 7 mm (Increment I, Fig. 8). Under further loading, the kinked cracks propagated towards the rear edge of the specimen along the 75° fibre direction (Increment II: Point 4, Fig. 8), and additional kinking events took place (Increment II: Point 5, Fig. 8). After the initial kinking events in the rear side region (Increment I: Points 1, 2 and 3, Fig. 8), the subsequent kinking events occurred closer to the front side region of the specimen, as shown by Point 5 in Increment II, Fig. 8. The area close to the front edge of the specimen (Increment II: Point 6, Fig. 8) was the last part of the specimen to kink and migrate, which occurred in Point 7, in Increment III, Fig. 8 (corresponding to the edge view of the same increment in Fig. 7). Completion of delamination migration in the rear side region (Increment II: Point 4, Fig. 8) and in the front side region (Increment III: Point 7, Fig. 8) of the specimen was produced by two independent kinking events, started at different locations inside the specimen.

X-ray CT scan results were confirmed by SEM inspection of previously tested specimens. SEM images in Fig. 9 reveal that delamination propagated close to the lower 0° ply at the interface, immediately after onset from the PTFE insert front, following the 0° fibre direction. Fig. 9b and c show SEM images of the lower and the upper delamination fracture surface, respectively, in the area close to the PTFE insert front. The lower fracture surface is fibre dominated, and shows fibres from the 0° ply, visible in Fig. 9b, while the upper fracture surface (75° ply) is matrix dominated, and shows imprints of the 0° fibres (Fig. 9c). This observation confirms that, at onset, delamination propagated close to the lower side of the interface, skimming the top of the 0° ply, driven by the negative shear stress sign. The shear cusps orientation in this area suggests that delamination propagated along the 0° fibre direction (see magnified details B and C in Fig. 9b and c, respectively). This behaviour is also evident in the front side region of the specimen (Fig. 9d), while in the rear side region delamination transitioned towards the upper ply at the interface and started to propagate inside the upper ply block, as indicated by the 75° fibres visible in the microphotograph of the lower fracture surface (0° ply) in Fig. 9e. The transition indicates that the principal stress plane at the delamination front is oriented so that delamination is driven towards the upper ply at the interface. An SEM image of

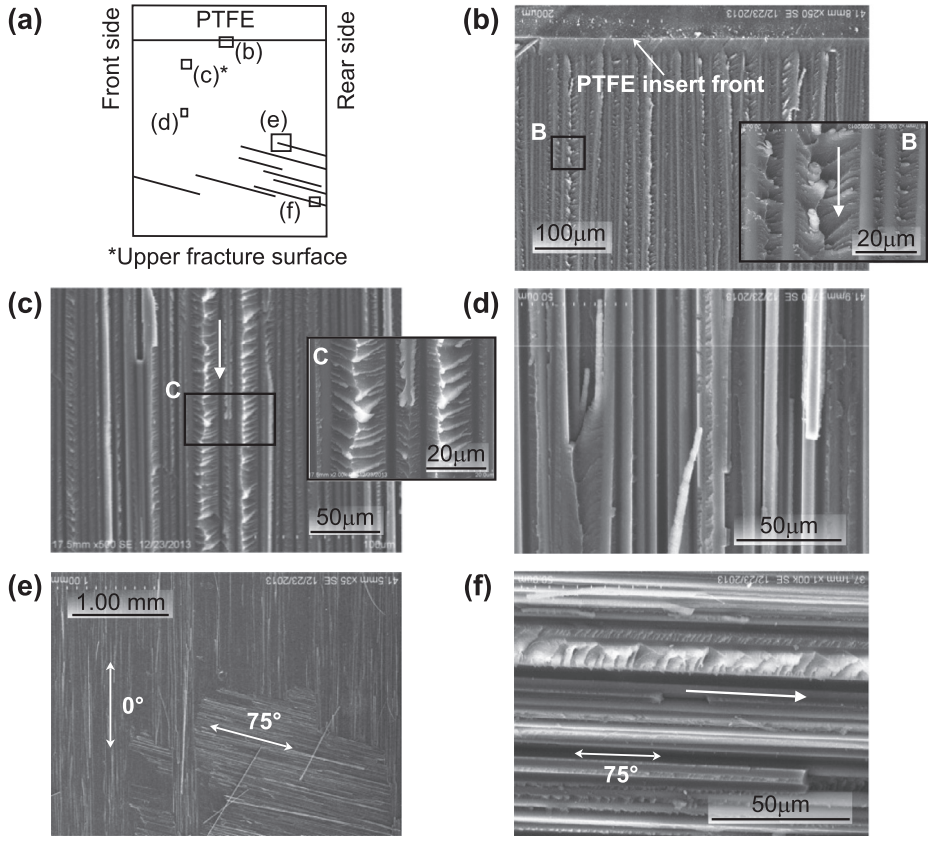

Fig. 9. SEM images of the lower (0°) delamination surface (except c) in a specimen containing a 0/75 interface loaded at $L = a_0$.

the kinked crack in the rear side region of the specimen is shown in Fig. 9f. The orientation of the shear cusps on the kinked crack surface suggests that the kinked crack propagated across the width of the specimen, following the 75° fibre direction, towards the rear edge of the specimen. However, this evidence is not conclusive, as fibre bridging between the surfaces of an intraply crack may result in local crack growth. Nevertheless, it is worth noticing that the direction of propagation inferred from the shear cusps and that obtained by X-ray CT scan are in agreement.

In some cases, kinked cracks propagated in the interior of a specimen and arrested when they reached the upper 75/0 interface, without causing delamination at this interface. This is likely because the local stress state did not favour turning the kinked crack into the 75/0 interface and/or there was insufficient crack driving force to initiate delamination. In other cases, the kinked cracks arrested prior to reaching the upper 75/0 ply interface. Two possible mechanisms are thought to be responsible for this behaviour. First, X-ray CT scan (Fig. 8) inspection revealed that once initiated, kinked cracks propagated along the 75° fibre direction, which could decrease crack driving force needed to continue propagating the kinked crack up through the ply stack. Second, the crack driving force of a kinked crack may diminish as it approaches near the upper 75/0 ply interface due to the stiffening effect of the 0° ply towards which the kinked crack is headed. Analogous observations have been made regarding crack growth in a material towards a stiffer substrate material [34,35].

The results from the numerical model, Figs. 5 and 6, provide further insight into the sequence of events, and overall damage morphology, observed in the initial stages of the test. The numerical results show that, at delamination onset ($\Delta a = 0$), the shear stress at the 0/75 interface has a sign (denoted here as negative), which would tend to drive the delamination towards the lower portion of the laminate (Fig. 3a). This correlates well with the fractographic observations, where delamination was seen to skim the 0° ply as it grew from the PTFE insert front and propagated following the 0° fibre direction.

The distance along the specimen, Δa_k, between the initiation of kinking in the interior of the specimen and the load-application point (Increment I: Point 1, Fig. 8) also correlates well with the location of the shear stress sign reversal computed by the numerical analysis (Figs. 5b and 6b). This confirms the hypothesis that, as delamination propagates, the principal stress plane rotates due to the shear sign reversal, and delamination is driven to propagate closer to the upper ply at the interface and eventually within it. It is important to highlight that the numerical results show that, contrary to the 0/90 interface case, shear sign reversal does not occur uniformly across the specimen width. Fig. 6b shows that the shear stress sign reverses at a lower delamination length nearest the rear edge of the specimen ($y = 7/8W$), while in the rest of the specimen width the shear sign has not yet changed, and therefore conditions are not favourable for kinking. Once again, this result correlates well with the observation that the first occurrences of crack kinking were registered in a portion of the specimen between the centre and the rear edge of the specimen (Increment I, Fig. 8). As the delamination grows, the shear sign eventually reverses over the entire width of the specimen, Fig. 5b, indicating delamination migration is favoured across the specimen width. This result also correlates well with the subsequent kinking events, which occured closer to the specimen front side, upon further loading, (Increment II: Point 5 and Increment III: Point 7, Fig. 8).

Measurements of kink angle, Ω (Fig. 7), were taken on the specimen edges. Kinking of delamination always initiated gradually from the 0/75 interface, with a smooth connection to the lower ply, and terminated suddenly at the next 75/0 interface, (similar observations were made in the cross-ply specimens [21]). Kink

angle ranged between 60° and 70° on the front edge and between 54° and 67° on the rear edge. An average kink angle of 61° was reported in cross-ply migration specimens [21]. In general, the kink angle on the front edge was greater than that on the rear edge. However, significant scatter in the data (with a standard deviation equal to 9°) precludes the formulation of a meaningful reason for this difference.

4.2.1.2. 0/60 ply interface. Representative single-step and incremental force–displacement responses of a 0/60 specimen loaded coincident with the PTFE insert front are shown in Fig. 10. Similar to the 0/75 interface, delamination onset from the PTFE insert front occurred during an unstable event (starting at the maximum load of 257 N in Fig. 10), followed by 5–12 mm of delamination propagation. As in the 0/75 case, Fig. 7, only edge views from the incremental test are shown, as they were equivalent to the single-step tests. More fibre bridging than in the 0/75 case was observed on both edges after delamination onset from the PTFE insert front in all the 0/60 specimens. The specimen response continued as described in the previous Section, with kinking events visible on the rear edge before the final migration. Specimen unloading was slightly non-linear, resulting in a residual machine crosshead displacement of just less than 0.2 mm.

The edge views suggested that delamination propagated differently along the front and the rear side of the specimen. On the front edge, delamination seemed to propagate at the 0/60 interface (Increment II, front view, Fig. 10) until it kinked into the 60° ply stack (Increment III, front view, Fig. 10) and migrated to the top 60/0 interface (Increment IV, front view, Fig. 10). On the rear edge, migration (Increment IV, rear view, Fig. 10) was preceded by a series of kinking events (Increments II and III, rear view, Fig. 10), after which the kinked cracks arrested turning back to the original 0/60 interface, and delamination continued to propagate. In the 0/60 specimens, this process was more evident than in the 0/75 specimens.

A sequence of X-ray CT scan images taken after each of the four loading increments (labelled I, II, III and IV in Fig. 10) is presented in Fig. 11. After initial unstable delamination growth onset, the edge views showed that the delamination grew uniformly at the 0/60 interface on both edges of the specimen, (Increment I,

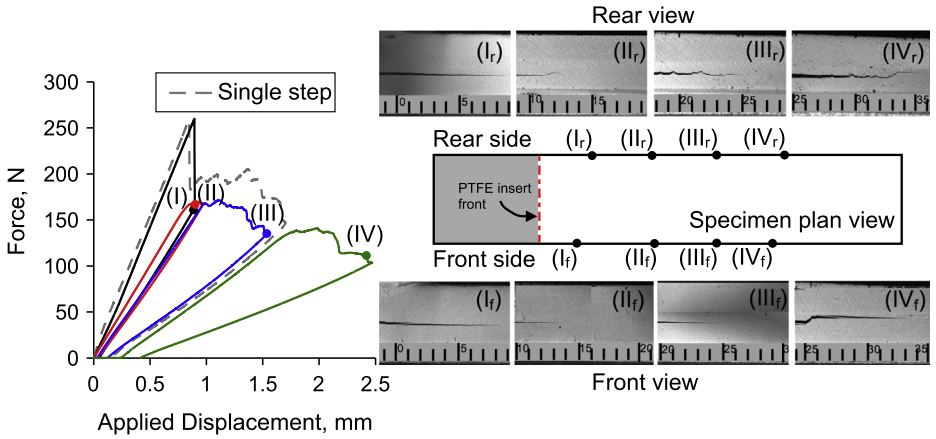

Fig. 10. Force–displacement response of specimens containing a 0/60 interface loaded at $L = a_0$ and edge views at key stages during the test, of the front edge of the specimen ("Front view") and the rear edge of the specimen ("Rear view").

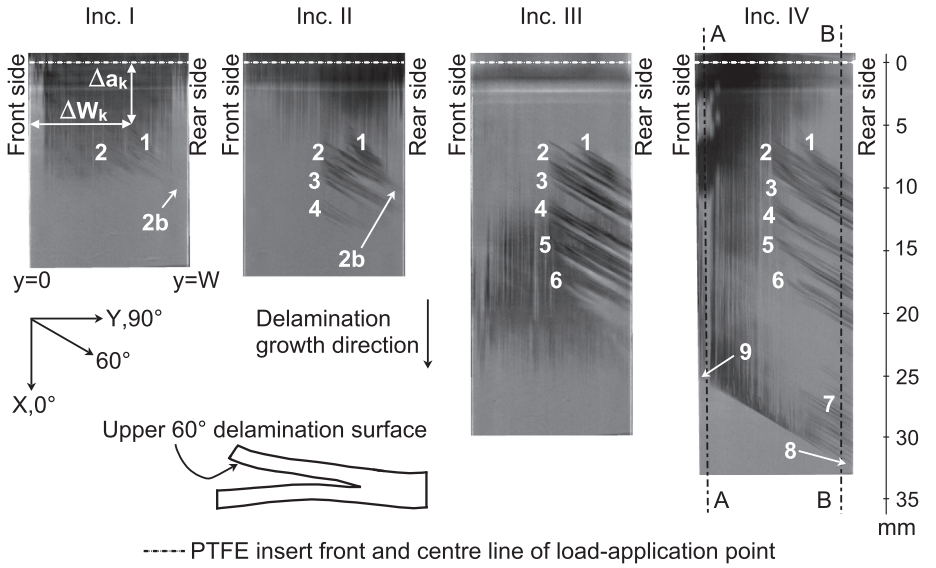

Fig. 11. Sequence of X-ray CT scan images of the upper delamination surface at the 0/60 interface resulting from incremental loading of a specimen. Sections A–A and B–B are shown in Fig. 12.

Fig. 10). The corresponding X-ray CT image (Increment I, Fig. 11) revealed that, although not visible from the edge views, kinking events took place at several locations within the specimen, as indicated by Points 1 and 2 in Increment I, Fig. 11. The resulting cracks propagated along the 60° fibre direction towards the rear edge of the specimen (similar to what was discussed before for the 0/75 case), but they did not reach the edge at this stage of testing (Increment I: Point 2b, Fig. 11). The initiation of kinking took place at a distance ΔW_k from the front edge of the specimen ranging between 7 and 11 mm and a distance Δa_k from the load-application point ranging between 4 and 10 mm (see Increment I, Fig. 11).

Analysing the X-ray CT scan images at consecutive increments revealed that the kinked cracks formed inside the specimen and propagated along the 60° fibre direction towards the rear edge of the specimen (Increments I and II: Point 2b, Fig. 11) until they became visible on the rear edge (Increment II, rear view, Fig. 10). Further loading caused additional kinking events in the rear side region of the specimen (Increments II, III and IV: Points 3–6, Fig. 11), which were also visible on the rear edge (see Increment III, rear view, Fig. 10). This result differs from the 0/75 case, where kinking events were observed at the rear side initially, and progressively closer to the front side upon further loading. Instead, in the 0/60 case, the delamination surface observed through X-ray can be divided in two regions exhibiting different features: a "front side region", exhibiting lines aligned to the 0° fibre direction, and a "rear side region", characterized by oblique lines, aligned to the 60° fibre direction (Increment IV, Fig. 11). This observation can be correlated to a higher variation in shear stress across the width present in the 0/60 specimens (Fig. 5c) which leads to the shear sign reversing first in the rear side region. This provides further evidence of the direct correlation between the inversion of the sign of the shear component τ_{23} and propensity for migration.

As in the 0/75 and 0/90 [21] case, kinking of delamination initiated gradually from the 0/60 interface, with a smooth connection with the lower ply, and terminated suddenly at the next 60/0 interface. Also similar to the 0/75 case, often kinked cracks arrested within the 60° ply stack, before reaching the upper 60/0 interface, or when they reached the upper 60/0 interface, without causing delamination at this interface (the mechanisms described in the previous section are thought to also be responsible for the observed behaviours). Delamination on the rear side region continued to propagate skimming the 60° ply stack and kinking through it (Increment IV: Point 7, Fig. 11). Ultimately, delamination migrated to the upper 60/0 interface in the rear side region of the specimen, when one of the kinked cracks caused delamination onset at the new interface (Increment IV: Point 8, Fig. 11). This corresponds to the rear edge view in the same increment in Fig. 10. In the front side region, delamination propagated almost uniformly at the 0/60 interface, skimming the lower 0° ply, until one single kinking event (Increment IV: Point 9, Fig. 11) and subsequent delamination migration took place, as appeared in the front edge view corresponding to Increment IV in Fig. 10. As observed in the 0/75 case, completion of delamination migration across the specimen was produced by two independent kinking events in the front side region (Increment IV: Point 9, Fig. 11) and in the rear side region (Increment IV: Point 8, Fig. 11) of the specimen.

Fig. 12 shows two X-ray CT images of the specimen along its length direction, in the front side region (Fig. 12a) and in the rear side region (Fig. 12b) of the specimen. These images correspond to section A–A and section B–B in Fig. 11 (Increment IV). Details in the figure show that the kinked cracks in the two regions of the specimen have a different profile. Kink angle ranged between 45° and 60° on the front edge and between 50° and 70° on the rear edge. An average kink angle of 61° was reported in cross-ply migration specimens [21]. In general, the kink angle on the front edge was smaller than that on the rear edge, which is in opposition to that which was observed in the 0/75 specimens. In Fig. 12a, the fibre bridging observed on the specimen edges at the delamination onset (as described at the beginning of this Section) is also visible. Fig. 12b provides a detail of the profile of the arrested kinked cracks in Points 4, 5 and 6 at Increment IV in Fig. 11 in the rear side region of the specimen, before migration was completed.

4.2.2. Effect of load-application point on damage events (0/60 and 0/75 ply interfaces)

Variation of the load-application point along the specimen has a similar effect on the two ply interfaces tested. Representative force–displacement responses of specimens loaded at load offset $L = \{0.35a_0, 1.1a_0, 1.2a_0, 1.3a_0\}$ are shown in Figs. 13 and 14 of specimens containing a 0/75 and a 0/60 interface, respectively. Figures also contain images of edge views of specimens at key stages during testing. Figs. 15 and 16 show X-ray CT images of specimens tested at each load offset, containing a 0/75 interface and a 0/60 interface, respectively.

In general, specimen response, delamination propagation and migration mechanisms were similar to those observed in specimens loaded at $L = a_0$. All the specimens exhibited delamination growth prior to migration, except those loaded on the delaminated

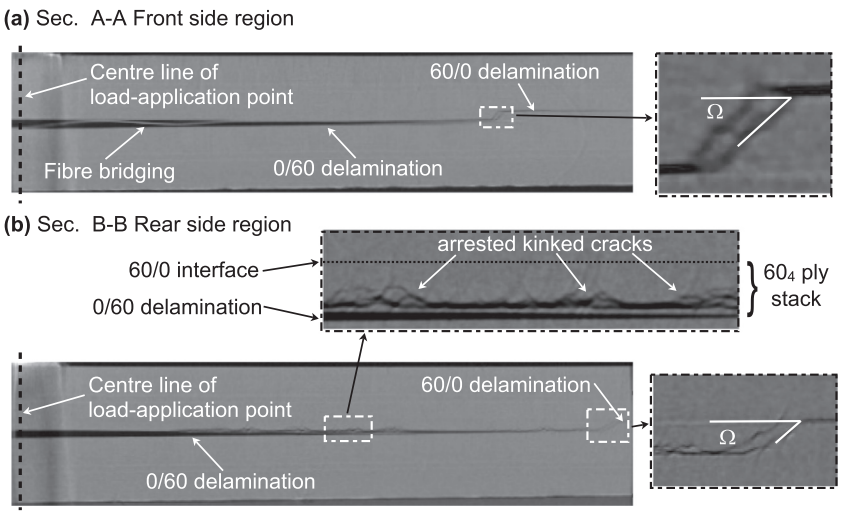

Fig. 12. Longitudinal sections showing the kinked cracks in the front (a) and in the rear (b) region of the specimen in the locations indicated in Increment IV, Fig. 11.

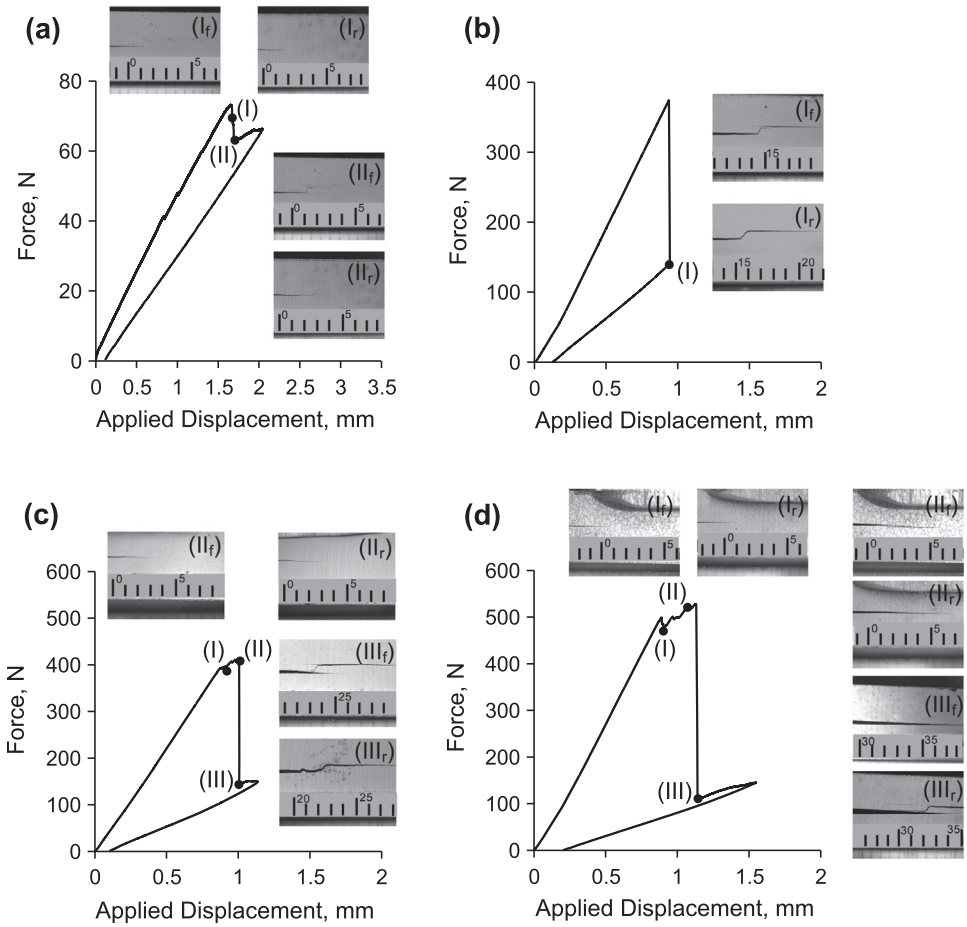

Fig. 13. Force–displacement response of specimens containing a 0/75 interface tested at load offset (a) $L = 0.35a_0$, (b) $L = 1.1a_0$, (c) $L = 1.2a_0$ and (d) $L = 1.3a_0$ and edge views at key stages during the test.

portion ($L = 0.35a_0$), in which the shear stress sign is favourable for kinking from the beginning of the test. Specimens loaded with load offsets $L = 1.2a_0$ and $L = 1.3a_0$ exhibited a small load drop, Point (I) in Figs. 13c, 13d, 14c and 14d, (not observed in case of $L = 1.1a_0$ in Figs. 13b and 14b) followed by a region of stable delamination growth, during which load continued to increase up to a maximum, before the main unstable event took place. The region of stable delamination propagation corresponded to 9–11 mm of delamination growth. During the initial phase of stable propagation, delamination tended to gradually turn towards the lower ply at the interface, because of the effect of the shear stress. As delamination was driven towards the 0° ply, it produced bundles of fibres which bridged the two plies at the interface, similar to those shown in Fig. 12a in a section close to the front edge of a specimen loaded at $L = a_0$. At higher load offsets, the fibre bridging extended from the PTFE insert front beyond the load-application point, where the shear stress sign reverses. The bridging fibres created resistance to delamination propagation which resulted in a continued increase of load during the stable delamination growth. Examples of this apparent resistance effect can be seen between Points (I) and (II) in Figs. 13d and 14d. Figs. 15 and 16 compare the X-ray images of the interfaces as a function of the load offset, L, for the specimens containing 0/75 and 0/60 interfaces, respectively. The migration locations on the specimen edges are labelled "F" and "R". As in case of specimens tested at load offset $L = a_0$, migration on the specimen edges was caused by independent kinking events, that started at different locations inside the specimen. Analysing both figures, it is evident that increasing the load offset, L, leads to an increase in the distance between migration location and the PTFE insert front. In some of the specimens tested with a load offset greater than a_0, kinking was visible only on the rear edge of the specimen and not on the front edge before the test was stopped, as can be seen in point B in Figs. 15e and 16d. In these cases, X-ray CT inspection showed that kinking occurred inside the specimen, away from the edges.

For specimens loaded at $L = 0.35a_0$, kinking and migration were observed directly at the location of the PTFE insert front. Migration was initially visible on the front edge of the specimen, (Point (I) in Figs. 13a and 14a). In specimens containing a 0/75 interface, upon further loading, migration was observed on the rear side of the specimens (Point (II) in Fig. 13a). In specimens containing a 0/60 interface, stable delamination growth was observed on the rear edge of the specimen (Point (II) in Fig. 14a), prior to completely migrating (Point (III) in Fig. 14a). SEM images of a specimen containing a 0/60 interface and loaded at $L = 0.35a_0$ are shown in Fig. 17. Images reveale that, in the rear side region, delamination propagated within the upper ply at the interface from the onset (PTFE insert front). Evidence of this is provided by the fibres oriented at 60° visible on the lower delamination surface (0° ply) in the rear side region of the specimen in Fig. 17a (locations shown in Fig. 17b–f are indicated in Fig. 17a). The image also shows the kinked crack directly at the PTFE insert front location. This result is in agreement with the shear stress sign, which tends to drive delamination towards the upper ply at the interface from the start of the test in this loading condition. Higher magnification images of the 0/60

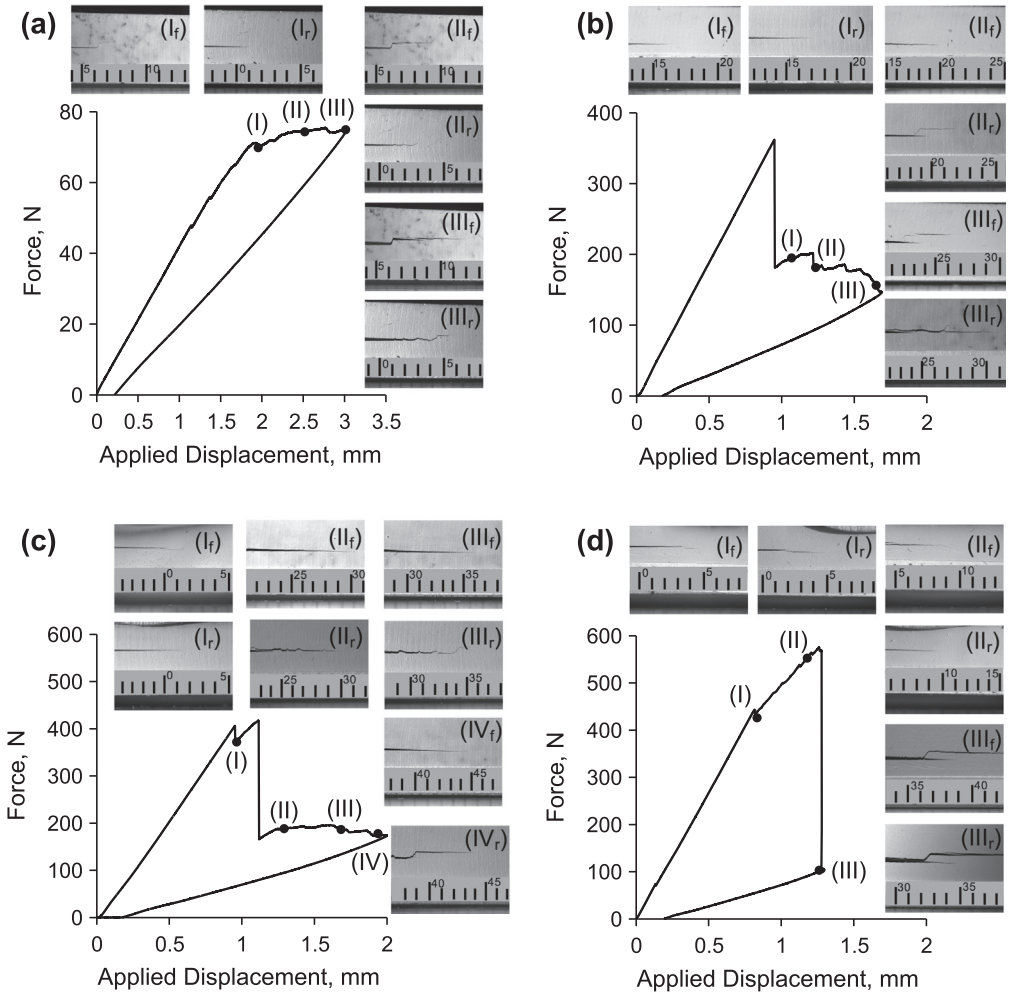

Fig. 14. Force–displacement response of specimens containing a 0/60 interface tested at load offset (a) $L = 0.35a_0$, (b) $L = 1.1a_0$, (c) $L = 1.2a_0$ and (d) $L = 1.3a_0$ and edge views at key stages during the test.

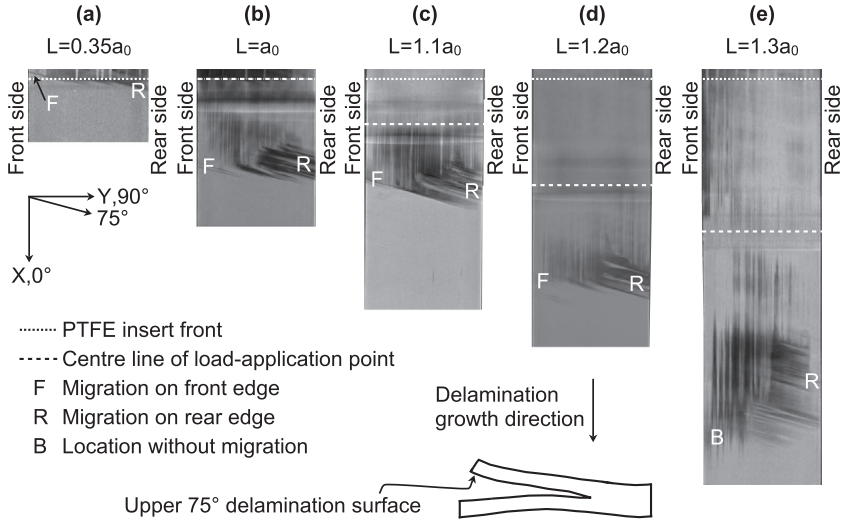

Fig. 15. X-ray CT scan images of the upper delamination surface of specimens containing a 0/75 interface tested at load offset (a) $L = 0.35a_0$, (b) $L = a_0$, (c) $L = 1.1a_0$, (d) $L = 1.2a_0$, (e) $L = 1.3a_0$.

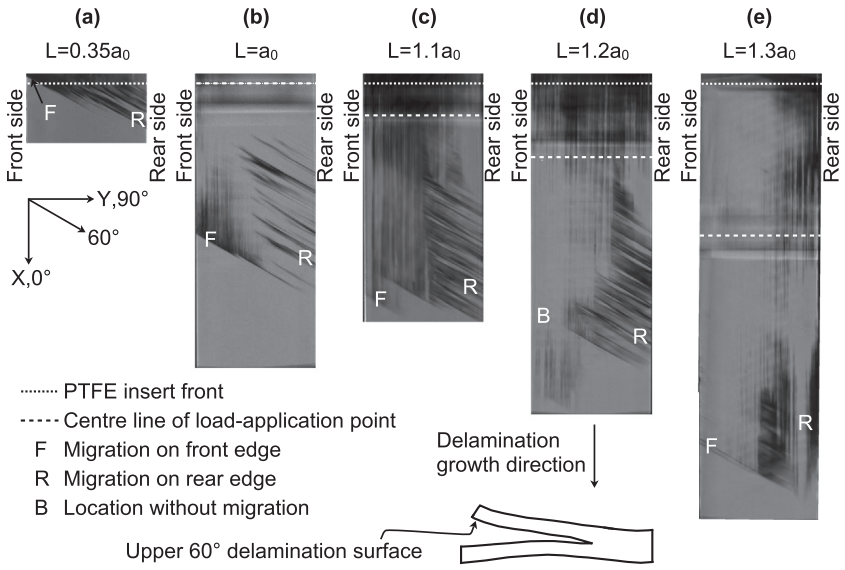

Fig. 16. X-ray CT scan images of the upper delamination surface of specimens containing a 0/60 interface tested at load offset (a) $L = 0.35a_0$, (b) $L = a_0$, (c) $L = 1.1a_0$, (d) $L = 1.2a_0$, (e) $L = 1.3a_0$.

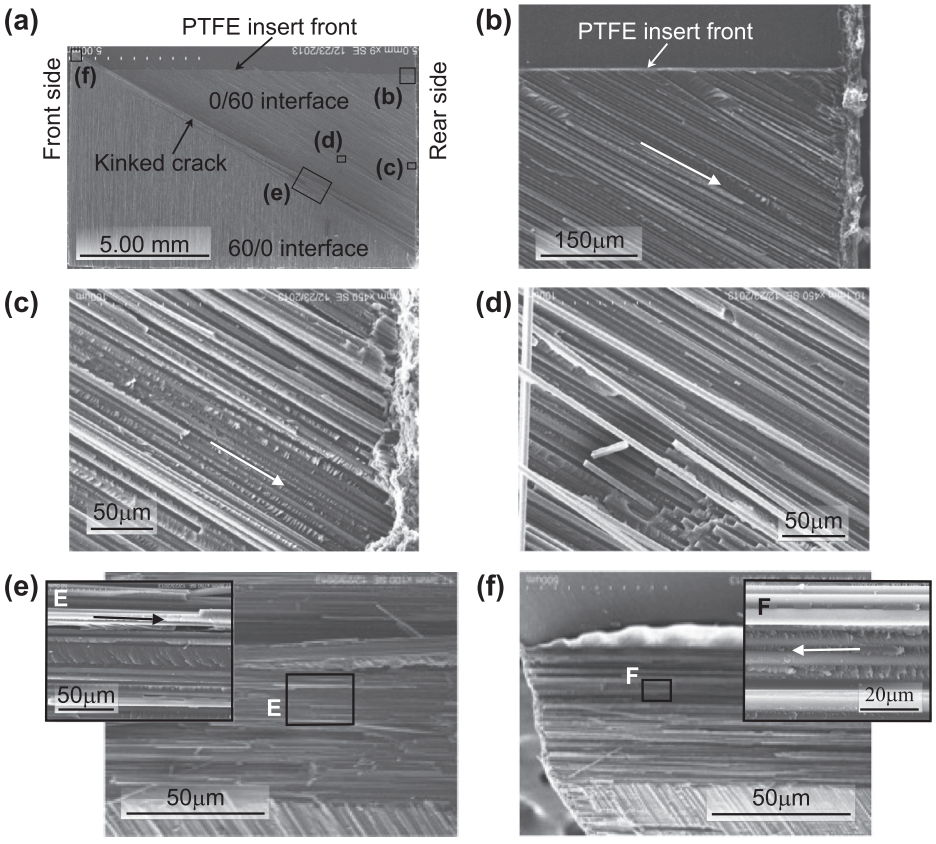

Fig. 17. SEM images of the lower (0°) delamination surface in a specimen containing a 0/60 interface tested at load offset $L = 0.35a_0$.

delamination surface in the rear side region of the specimen are shown in Fig. 17b, near the PTFE insert front, and in Fig. 17c and d in the location indicated in Fig. 17a. Fig. 17e and f show SEM images of the kinked crack inside the specimen in the rear side region, and on the front edge, respectively. The shear cusps orientation along the kinked crack, along with evidence from the X-ray CT scan inspection, suggests that kinking occurs in the interior of the specimen and the kinked crack propagates in the specimen width along the θ fibre orientation towards the edges of the specimen.

5. Summary

A delamination migration test was combined with a novel specimen design to investigate delamination propagation and migration at generic 0/θ ply interfaces. Specimens containing a 0/60 and 0/75 ply interface were studied. The main characteristics of delamination migration at a 0/θ interface can be summarized as follows:

1. *Shear stress sign*: kinking of delamination out of the initial 0/θ interface is only possible if the sign of the component of the interlaminar shear stress in the direction transverse to the θ-oriented fibres is such that the delamination is driven into the θ ply. The favourable sign of the shear stress is a condition necessary for migration.
2. *Shear stress distribution*: shear stress distribution along the delamination front at a 0/θ interface is not uniform, but varies across the specimen width, depending on the fibre angle, θ, at the interface. Therefore, as delamination propagates, rotation of the principal stress and, ultimately, the shear stress sign reversal, varies across the specimen width.
3. *Delamination propagation*: delamination growth at the 0/θ interfaces studied tends to grow closer to the lower 0° bounding ply.
4. *Kinking*: kinking initiates in the specimen in a location which depends upon the shear stress distribution, and, therefore, upon the fibre angle. Once delamination kinks out of the 0/θ interface, it can propagate through the entire θ-oriented ply stack or turn back to the original interface, depending on which option is energetically favourable. The kinked cracks propagate along the fibre direction in the θ-oriented ply stack.
5. *Migration*: delamination migration is achieved by multiple independent kinking events across the specimen width, which start in the interior of the specimen and propagate towards one of the edges and through the thickness of the specimen, ultimately leading to the relocation of the delamination at a new interface.

6. Concluding remarks

Correlation between the numerical results and experimental observations demonstrates that the shear stress sign at the delamination front, combined with the fibre direction of the bounding plies, dictates whether delamination will propagate near the interface along the ply direction, or migrate through the neighbouring ply. Furthermore, it was observed that delamination propagation at a non-unidirectional ply interface does not proceed precisely at the midplane of the interface, but it tends to grow closer to one of the bounding plies, depending on the sign of the shear stress. These results demonstrate that the migration process is inherent to delamination between plies of dissimilar orientation, and it may thus be necessary to account for it in the simulation of damage propagation in tape laminates. Experimental results presented here provide validation data for modelling strategies aimed at capturing delamination migration.

The knowledge acquired through this work can be extended to other cases where delamination migration is known to occur in a similar manner, such as skin/stringer structural elements subjected to flexural loading or the "spiral stair case" damage configuration in composite laminates subjected to low-velocity impact. Furthermore, better understanding and simulation of delamination propagation and migration at non-unidirectional ply interfaces can be exploited in damage tolerant design, where migration can be promoted to stop or re-direct delamination, or as an energy dissipating mechanism.

Acknowledgements

This material is based on work supported by the National Aeronautics and Space Administration (NASA), Langley Research Center, United States, under Research Cooperative Agreement No. NNL09AA00A. The first author is supported by the Engineering and Physical Sciences Research Council (EPSRC), United Kingdom, through the Centre for Doctoral Training in Advanced Composites [grant number EP/G036772/1]. Special thanks to Drs. T.K. O'Brien, J. Reeder, M. Czabaj and W. Jackson of NASA and Prof P. Weaver of ACCIS, for the invaluable technical discussions.

References

[1] Robinson P, Song DQ. A modified DCB specimen for mode I testing of multidirectional laminates. J Compos Mater 1992;26:1554–77.
[2] Andersons J, König M. Dependence of fracture toughness of composite laminates on interface ply orientations and delamination growth direction. Compos Sci Technol 2004;64:2139–52.
[3] ASTM D 5528-13. Standard test method for mode I interlaminar fracture toughness of unidirectional fiber-reinforced polymer matrix composites. In: Annual Book of ASTM Standards, vol. 15.03. American Society for Testing and Materials; 2014.
[4] ASTM D 6671-13. Standard test method for mixed mode I-mode II interlaminar fracture toughness of unidirectional fiber-reinforced polymer matrix composites. In: Annual Book of ASTM Standards, vol. 15.03. American Society for Testing and Materials; 2014.
[5] ASTM D 6115-97. Standard test method for mode I fatigue delamination growth onset of unidirectional fiber-reinforced polymer matrix composites. In: Annual Book of ASTM Standards, vol. 15.03. American Society for Testing and Materials; 2014.
[6] Turon A, Dávila CG, Camanho PP, Costa J. An engineering solution for mesh size effects in the simulation of delamination using cohesive zone models. Eng Fract Mech 2007;74:1665–82.
[7] Rybicki EF, Kanninen MF. A finite element calculation of stress intensity factors by a modified crack closure integral. Eng Fract Mech 1977;9(4):931–8.
[8] Hull D, Shi YB. Damage mechanisms characterization in composite damage tolerance investigations. Compos Struct 1993;23:99–120.
[9] Krueger R, Cvitkovich MK, O'Brien TK, Minguet PJ. Testing and analysis of composite skin/stringer debonding under multi-axial loading. J Compos Mater 2000;34(15):1263–300.
[10] Greenhalgh ES, Singh S. Investigation of the failure mechanisms for delamination growth from embedded defects. In: Proceedings of ICCM12, Paris, France; 1999.
[11] Hallett SR, Green BG, Jiang WG, Wisnom MR. An experimental and numerical investigation into the damage mechanisms in notched composites. Compos Part A – Appl Sci 2009;40:613–24.
[12] Canturri C, Greenhalgh ES, Pinho ST, Nilsson S. Delamination growth mechanism from embedded defects in compression. In: Proceedings of ICCM18, Jeju Island; 2011.
[13] Tao J, Sun CT. Influence of ply orientation on delamination in composite laminates. J Compos Mater 1998;32:1933–47.
[14] Belytschko T, Gracie R, Ventura G. A review of extended/generalized finite element methods for material modeling. Model Simul Mater Sc 2009;17(4):1–24.
[15] Ling D, Yang Q, Cox B. An augmented finite element method for modeling arbitrary discontinuities in composite materials. Int J Fract 2009;156(1):53–73.
[16] van der Meer FP, Sluys LJ. A phantom node formulation with mixed mode cohesive law for splitting in laminates. Int J Fract 2009;158:107–24.
[17] Chen BY, Pinho ST, De Carvalho NV, Baiz PM, Tay TE. A floating node method for the modelling of discontinuities in composites. Eng Fract Mech 2014;127:104–34.
[18] Tay TE, Sun XS, Tan VBC. Recent efforts toward modelling interactions of matrix cracks and delaminations: an integrated XFEM-CE approach. Adv Compos Mater 2014;23(5–6):391–408.
[19] Canturri C, Greenhalgh ES, Pinho ST, Ankersen J. Delamination growth directionality and the subsequent migration process – the key to damage tolerant design. Compos Part A – Appl Sci 2013;54:79–87.
[20] Greenhalgh ES, Rogers C, Robinson P. Fractographic observations on delamination growth and the subsequent migration through the laminate. Compos Sci Technol 2009;69:2345–51.
[21] Ratcliffe JG, Czabaj MW, O'Brien TK. A test for characterizing delamination migration in carbon/epoxy tape laminates. National Aeronautics and Space Administration Technical Memorandum, NASA/TM – 2013–218028; 2013.
[22] Ratcliffe JG, De Carvalho NV. Investigating delamination migration in composite tape laminates. National Aeronautics and Space Administration Technical Memorandum, NASA/TM – 2014–218289; 2014.
[23] He MY, Hutchinson JW. Kinking of a crack out of an interface. J Appl Mech 1989;56(2):270–8.
[24] Purslow D. Matrix fractography of fibre reinforced epoxy composites. Composites 1986;17(4):289–303.

[25] O'Brien TK. Composite interlaminar shear fracture toughness, G_{IIC}: shear measurement or sheer myth? In: Bucinell RB, editor. Composite Materials: Fatigue and Fracture, (Seventh Volume), ASTM STP, 1330. Philadelphia: American Society for Testing and Materials; 1998. p. 3–18.
[26] Greenhalgh ES. Failure analysis and fractography of polymer composites. Cambridge: Woodhead Publishing; 2009.
[27] De Carvalho NV, Chen BY, Pinho ST, Ratcliffe JG, Baiz PM, Tay TE. Modeling delamination migration in cross-ply tape lamiantes. Compos Part A - Appl Sci 2015;71:192–203.
[28] Jones MJ. Mechanics of composite materials. Taylor and Francis; 1999.
[29] Davidson BD, Krueger R, König M. Effect of stacking sequence on energy release rate distributions in multidirectional DCB and ENF specimens. Eng Fract Mech 1996;55(4):557–69.
[30] Sun CT, Zheng S. Delamination characteristics of double-cantilever beam and end-notched flexure composite specimens. Compos Sci Technol 1996;56:451–9.
[31] Hexcel Corporation. HexPly® 8552 Product Data Sheet. <http://hexcel.com>; 2007.
[32] ABAQUS®/Standard Ver. 6.12 User's Manual; 2012.
[33] O'Brien TK, Krueger R. Analysis of flexure tests for transverse tensile strength characterization of unidirectional composites. J Compos Technol Res 2003;25:50–68.
[34] Cook TS, Erdogan F. Stresses in bonded materials with a crack perpendicular to the interface. Int J Eng Sci 1972;10:677–97.
[35] He MY, Hutchinson JW. Crack deflection at an interface between dissimilar elastic materials. Int J Solids Struct 1989;15(9):1053–67.